3. H. K. Mao *et al.*, *Science* **239**, 1131 (1988).
4. R. J. Hemley and H. K. Mao, *Phys. Rev. Lett.* **61**, 857 (1988).
5. K. Inoue, H. Kanzaki, S. Suga, *Solid State Comm.* **30**, 627 (1979).
6. P. S. Hawke *et al.*, *Phys. Rev. Lett.* **41**, 994 (1978).
7. L. F. Vereschagin, Y. N. Yakolev, Yu. A. Timofeev, *JETP. Lett.* **21**, 85 (1975); N. Kawai, M. Togaya, O. Mishima, *Proc. Japan. Acad.* **51**, 630 (1975).
8. A. Jayaraman, *Rev. Mod. Phys.* **55**, 65 (1983); A. P. Jephcoat, H. K. Mao, P. M. Bell, in *Hydrothermal Experimental Techniques*, G. C. Ulmer and H. L. Barnes, Eds. (Wiley Interscience, New York, 1987), p. 469–506; H. K. Mao, in *Simple Molecular Systems at Very High Densities*, P. Loubeyre and A. Polian, Eds. (Plenum, New York, 1988), pp. 221–236.
9. H. K. Mao, P. M. Bell, J. W. Shaner, D. J. Steinberg, *J. Appl. Phys.* **49**, 3276 (1978); H. K. Mao, J. Xu, P. M. Bell, *J. Geophys. Res.* **91**, 4673 (1986); P. M. Bell, J. Xu, H. K. Mao, in *Shock-Waves in Condensed Matter*, Y. Gupta, Ed. (Plenum, New York, 1986), pp. 125–130; R. J. Hemley *et al.*, *Phys. Rev. B*, in press.
10. H. K. Mao, P. M. Bell, R. J. Hemley, *Phys. Rev. Lett.* **55**, 99 (1985).
11. M. Cardona, in *Topics in Applied Physics*, M. Cardona and G. Guntherodt, Eds. (Springer-Verlag, New York, 1982), vol. 50, pp. 19–178. Because the hydrogen at very high pressures was typically in close proximity to the surface of the steel gasket, possible surface-enhanced Raman scattering from the hydrogen (manifestly pressure-induced) cannot be ruled out [M. Moskovitz, *Rev. Sci. Instrum.* **57**, 783 (1983)].
12. H. K. Mao and R. J. Hemley, *Bull. Am. Phys. Soc.* **34**, 836 (1989); R. J. Hemley and H. K. Mao, in preparation.
13. H. K. Mao *et al.*, in preparation.
14. H. K. Mao, R. J. Hemley, P. M. Bell, *Bull. Am. Phys. Soc.* **31**, 453 (1986).
15. Other explanations of the increase in absorption include possible effects caused by trace impurities in the hydrogen and possible pressure-induced chemical reactions between the hydrogen and the diamond at high pressures. At present, there is no evidence for either of these mechanisms. The starting material consisted of research grade normal hydrogen gas with a purity of 99.9995%. We have found no evidence for high-pressure chemical reactions between the sample and diamond at 77 K taking place over the time scale of these experiments. Following pressure release, no changes in the surface of diamonds in the regions exposed to the hydrogen have been observed. The darkening of the sample above 200 GPa could also be produced by Mie scattering from small particles (≤ 1 μm) of a new phase of hydrogen nucleating within the molecular phase. If so, the observed optical properties of the mixed-phase sample would initially be dominated by particle-size effects rather than bulk properties [see M. Born and E. Wolf, *Principles of Optics*, Sixth Edition (Pergamon, New York, 1980), pp. 633–664]. Such a mechanism is conceivable, for example, if nuclei of a highly conductive (monatomic) metallic phase were formed within the molecular phase. The evidence for molecular dissociation is discussed in the final paragraph of the article.
16. K. F. Herzfeld, *Phys. Rev.* **29**, 701 (1927). In this model, the molecular polarizability is assumed to be independent of density, and metallization is predicted to occur at the pressure at which the refractive index diverges. This model has also been applied to hydrogen by J. van Straaten and I. F. Silvera [*Phys. Rev. B* **37**, 1989 (1988)]. They used a different equation of state but obtained results that are similar to those reported here.
17. J. van Straaten and I. F. Silvera, *Phys. Rev. B* **37**, 6478 (1988).
18. C. Friedli and N. W. Ashcroft, *ibid.* **16**, 662 (1977). Band overlap was calculated to occur at 2.43 cm^3/mol in this study. This corresponds to a pressure of 170 GPa calculated with (T = 0 K) x-ray equation of state (*3*).
19. B. I. Min, H. J. F. Jansen, A. J. Freeman, *Phys. Rev. B* **33**, 6383 (1986). Band-overlap occurred at 170 (± 20) GPa according to the calculated equation of state. Local-density approximation methods used in this work typically underestimate band-gaps.
20. K. A. Goettel, J. H. Eggert, I. F. Silvera, W. C. Moss, *Phys. Rev. Lett.* **62**, 665 (1989); R. Reichlin *et al.*, *ibid.*, p. 669 (1989).
21. A. P. Jephcoat *et al.*, *ibid.* **59**, 2670 (1987).
22. R. Reichlin, M. Ross, S. Martin, K. A. Goettel, *ibid.* **56**, 2858 (1986).
23. J. H. Eggert, K. A. Goettel, I. F. Silvera, *Appl. Phys. Lett.* **53**, 2489 (1988).
24. K. A. Goettel, H. K. Mao, P. M. Bell, *Rev. Sci. Instrum.* **56**, 1420 (1985).

25. We thank L. C. Chen and J. Shu for help with the experiments and N. W. Ashcroft, W. A. Bassett, and an anonymous reviewer for constructive comments. We are grateful to the Carnegie Institution of Washington, the Division of Earth Sciences of NSF (grants EAR-8610068, EAR-8720326, and EAR-8708127), and NASA (grant NAGW214) for support.

21 April 1989; accepted 5 May 1989

Rates of Tectonometamorphic Processes from Rubidium and Strontium Isotopes in Garnet

JOHN N. CHRISTENSEN, JOHN L. ROSENFELD,* DONALD J. DEPAOLO

Measurement of the radial variation of the $^{87}Sr/^{86}Sr$ ratio in a single crystal from a metamorphic rock can be used to determine the crystal's growth rate. That variation records the accumulation of ^{87}Sr from radioactive decay of ^{87}Rb in the rock matrix from which the crystal grew. This method can be used to study the rates of petrological processes associated with mountain building. It is applied to garnet crystals in rocks from southeast Vermont that were metamorphosed about 380 million years ago. The average growth rate measured for three garnets is $1.4^{+0.92}_{-0.45}$ millimeters per million years and the average time interval of growth is 10.5 ± 4.2 million years. Garnet and its mineral inclusions provide a sequential record of temperature change, strain, and chemical reactions during metamorphism; therefore, the technique offers the potential for determination of the rates of those processes as well. The growth interval and observed amount of rotation recorded by inclusion trails in one garnet indicate that the mean shear strain rate during garnet growth was $2.4^{+1.6}_{-0.7} \times 10^{-14}$ per second.

FUNDAMENTAL TO AN UNDERSTANDING of metamorphism is knowledge of the rates of concurrent processes affecting the rocks such as heating, increase in pressure, devolatilization, deformation, and recrystallization. Quantitative measurement of these rates has proved elusive because continued metamorphism acts to overprint or to erase earlier metamorphic phenomena. We have overcome this difficulty by measuring the growth rate of a widespread metamorphic mineral, garnet, that commonly resists overprinting. We determine the growth rate by precisely measuring the radial variation of the $^{87}Sr/^{86}Sr$ ratio (*1*) in single crystals of garnet. This variation reflects the rate of accumulation of ^{87}Sr in the rock matrix caused by radioactive decay of ^{87}Rb during the time of growth of the garnet crystal.

We chose garnet because it grows by dehydration reaction during metamorphism in common rocks, because it preferentially incorporates Sr relative to Rb, and because its low cationic diffusivity (*2*) helps to preserve the isotopic record. Garnet also preserves other information important in characterizing metamorphism. For example, there is the possibility of estimating the pressure and temperature history of the rock during garnet growth from mineral inclusions in garnet (*3, 4*), oxygen-isotope thermometry (*5*), and chemical zoning profiles (*6*). Garnet can also record progressive deformation of its surrounding matrix (*7, 8*) because it is rigid, equant, and commonly inclusion-bearing. Thus measurement of growth rates of metamorphic garnet may provide a direct measure of rates of temperature-pressure change, chemical reaction, dehydration, and deformation during metamorphism.

Determination of the growth interval of a mineral by our method requires that (i) the mineral had a much lower $^{87}Rb/^{86}Sr$ ratio than the matrix from which it grew; (ii) changes in the $^{87}Sr/^{86}Sr$ ratio of the matrix were due solely to in situ decay of ^{87}Rb in the matrix and were not significantly influenced by infiltrating fluid or exchange with neighboring rock units with contrasting $^{87}Sr/^{86}Sr$ and $^{87}Rb/^{86}Sr$ ratios; (iii) the local source matrix sampled by the growing mineral was homogeneous with respect to $^{87}Sr/^{86}Sr$ and $^{87}Rb/^{86}Sr$ ratios during growth; (iv) Sr diffusion in the mineral was suffi-

J. N. Christensen and J. L. Rosenfeld, Department of Earth and Space Sciences, University of California, Los Angeles, CA 90024.
D. J. DePaolo, Berkeley Center for Isotope Geochemistry, Department of Geology and Geophysics, University of California, Lawrence Berkeley Laboratory, Berkeley, CA 94720.

*To whom correspondence should be addressed.

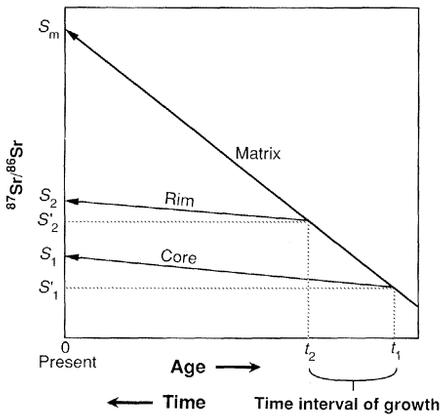

Fig. 1. Hypothetical plot of $^{87}Sr/^{86}Sr$ ratio versus age for a mineral growing continuously between times t_1 and t_2 from a matrix with a much higher $^{87}Rb/^{86}Sr$ ratio than that of the mineral. Shown are evolution lines for mineral core, mineral rim, and matrix. Slopes of evolution lines are proportional to their $^{87}Rb/^{86}Sr$ ratios. The $^{87}Rb/^{86}Sr$ ratio of the matrix and the difference in $^{87}Sr/^{86}Sr$ ratios of the core and rim determine time interval of growth.

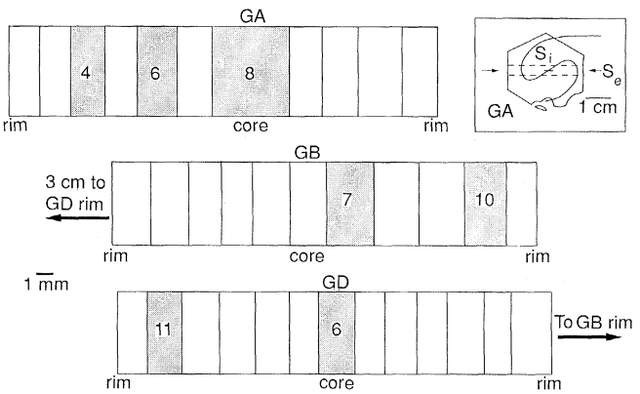

Fig. 2. Positions of analyzed segments (shaded) and unanalyzed segments for garnets GA, GB, and GD. Segments were approximately 5 mm tall. Inset: sketch, showing S-shaped arrangement of inclusions in garnet GA (S_i), indicating about 4 radians rotation during growth; S_e is the plane of foliation in the matrix.

ciently slow that redistribution of Sr within the mineral after its formation or between the mineral and matrix was negligible; (v) mineral growth did not significantly affect the $^{87}Rb/^{86}Sr$ ratio of the matrix. We show below that these requirements appear to be met by the garnets we have investigated.

If the above conditions are fulfilled, radial variation in the measured $^{87}Sr/^{86}Sr$ ratio, after correction for the decay of ^{87}Rb in the garnet subsequent to growth, records the Sr isotopic change in the matrix during growth (Fig. 1). This radial variation in turn gives the chronology of growth of the garnet. The initial value of the $^{87}Sr/^{86}Sr$ ratio at the time of formation of a particular segment, S'_g, is given by:

$$S'_g = \frac{R_g S_m - R_m S_g}{R_g - R_m} \quad (1)$$

where $^{87}Sr/^{86}Sr \equiv S$, $^{87}Rb/^{86}Sr \equiv R$, the subscript g is a numerical index of segments of a garnet crystal, and m refers to the matrix. All unprimed values are measured quantities. The time (at present, $t = 0$; absolute age $\equiv -t_g$) of formation of a segment is given by (*9*):

$$t_g = -\frac{1}{\lambda} \ln \left[\frac{S_g - S_m}{R_g - R_m} + 1 \right]$$

$$= -\frac{1}{\lambda} \ln \left[\frac{S'_g - S_m}{-R_m} + 1 \right] \quad (2)$$

The difference in the time of growth, $t_2 - t_1$, of a segment 1 and a later segment 2 can be determined with Eq. 2. Because the age of each segment is calculated using the same matrix values (S_m, R_m), the uncertainty in the age difference, $t_2 - t_1$, depends only on the uncertainties in S'_1 and S'_2 (*10*).

As a mineral with low $^{87}Rb/^{86}Sr$ ratio begins to grow from a matrix with high $^{87}Rb/^{86}Sr$ ratio, it incorporates Sr of isotopic composition S'_1 (Fig. 1). At a later time, t_2, the rim grows, incorporating Sr of isotopic composition S'_2 (Fig. 1), the isotopic composition having changed because of ^{87}Rb decay in the matrix. After crystallization both the rim and core follow evolution lines of smaller slope. Because these slopes are small and because the precision with which they can be measured is proportional to their absolute values (Table 1), the uncertainty in the initial isotope ratios is approximately the same as the uncertainty in the measured ratios.

The time resolution of the growth interval is directly proportional to the $^{87}Rb/^{86}Sr$ ratio of the matrix and largely independent of the absolute age of the crystal. We are able to resolve a difference of 4×10^{-5} in the $^{87}Sr/^{86}Sr$ ratio. For a matrix $^{87}Rb/^{86}Sr$ ratio of 10, this precision gives a resolution of 0.28 million years (m.y.) Typical $^{87}Rb/^{86}Sr$ ratios of garnet-bearing schist are between 1 and 100.

We analyzed three garnets (GA, GB, and GD) collected in southeast Vermont near the base of the late Cambrian (?) Ottauquechee Formation on the west side of the Athens dome. These garnets were chosen for their large size, relative paucity of inclusions, and because they preserve a record of deformation related to the Acadian Orogeny (*8*). Peak metamorphic temperatures in the rocks were about 500°C (staurolite zone). During the orogeny, the rocks were first transported to the west in a series of large nappes (*11*); they were later arched upward by a number of mantled gneiss domes including the Athens and Chester domes (*8*).

The garnets are large (3 cm) crystals in a schist containing paragonite, muscovite, chlorite, quartz, and plagioclase. Quartz, ilmenite, minor tourmaline, and small ($\leq$10 μm) clinozoisite inclusions are present in the garnets (*12*). The garnets have narrow alteration rims of muscovite, paragonite, and chlorite. Electron microprobe traverses of GB and GD indicate that the crystals are normally zoned in MnO, MgO, and FeO and that Mn is not enriched at the rims. There is no significant zoning in CaO in GB and GD except for a small decrease within 1 mm of the garnet edge. Rim samples were taken inward of this zone. In one of the analyzed garnets (GA), the inclusions are arranged (Fig. 2, inset) in a sigmoid spiral in a cross section. The pattern indicates that the garnet rotated during growth; rotation is inferred to have taken place during nappe

Table 1. Results of Rb and Sr analyses. Reported errors of the measured $^{87}Sr/^{86}Sr$ ratios are 2 SD of the mean of 20 to 30 sets of data, each set consisting of ten measurements of the $^{87}Sr/^{86}$ Sr ratio. The errors of the $^{87}Rb/^{86}Sr$ ratios of the garnet segments are based on the error of the concentrations derived from the isotopic analyses. The error of the $^{87}Rb/^{86}Sr$ ratios are a small contribution to the total error of the calculated time intervals (*10*); $(^{87}Sr/^{86}Sr)_0$ values are calculated ratios at the time of segment formation for matrix II (Eq.2).

Sample	Sr (ppm)	Rb (ppm)	$^{87}Rb/^{86}Sr$	$^{87}Sr/^{86}Sr$	$(^{87}Sr/^{86}Sr)_0$
GA-8	15.05	0.406	0.07810 ± 8	0.714635 ± 20	
GA-6	13.74	0.453	0.0955 ± 3	0.714792 ± 22	
GA-4	26.56	0.407	0.0443 ± 1	0.714535 ± 19	
GB-7	14.58	0.488	0.0968 ± 2	0.714545 ± 26	0.714038
GB-10	14.99	0.524	0.1012 ± 2	0.714648 ± 22	0.714127
GD-6	19.11	0.666	0.1009 ± 2	0.714397 ± 25	0.713851
GD-11	11.53	0.442	0.1110 ± 2	0.714593 ± 47	0.714008
		0.442			
Matrix I	246.1	69.47	0.8178 ± 2	0.718922 ± 22	
Matrix II	268.5	96.65	1.0432 ± 6	0.719498 ± 20	

emplacement (*8*). A mineral age of 376 ± 5.5 Ma (million years ago) (^{40}Ar-^{39}Ar total fusion, amphibole) has been obtained from nearby amphibolite (*13*). Another mineral age of 380 ± 2 Ma (^{40}Ar-^{39}Ar, incremental heating, amphibole) has been obtained from an amphibolite that was collected 50 m from our garnet sample location (*14*).

A disk was cut and polished through the center of each garnet perpendicular to a rotation axis (where determined) from oriented samples. A diameter-parallel prism was cut from each disk and wire-sawed into 2- to 3-mm-long segments for isotopic analysis (Fig. 2). The data (*15*) are thus an average for each segment, but because the garnets are large (~3 cm in diameter), the segments are short relative to garnet diameter. Garnets GB and GD were separated by ~3 cm. Sample GA was collected ~1 m distant from GB and GD parallel to the strike. We have analyzed core and rim segments from GB, GD, and GA and an intermediate segment from GA (Fig. 3). We also analyzed portions of matrix associated with GB and GD. Matrix I is a 6-g sample within 5 cm of GB and GD, and matrix II is a 100-g slab taken adjacent to the garnets. No unweathered matrix for GA was available.

The Sr concentrations in the analyzed garnet segments ranged from 11.5 to 26.5 ppm (Table 1); there was no consistent relation to radial position in the garnets. Concentrations of Sr in the matrix were 10 to 20 times as great as those in the garnets; Rb concentrations were up to 200 times as great. Growth of garnet in the schist therefore had little effect on the ^{87}Rb/^{86}Sr ratio of the matrix, satisfying the fifth condition above. The matrix ^{87}Rb/^{86}Sr values are ~1, which places the specimens at the low end of the range of time resolution. The ^{87}Rb/^{86}Sr ratios of the garnet segments are less than 0.1 times that of the matrix fulfilling the first condition.

For each garnet, there was a measurable difference in the ^{87}Sr/^{86}Sr ratio between core and rim. For GB and GD, the ^{87}Rb/^{86}Sr ratios of the core and rim segments are nearly equal, whereas for GA, the ^{87}Rb/^{86}Sr ratios are more variable (Fig. 3). The measured isotopic difference in ^{87}Sr/^{86}Sr between the core and rim segments is 1.0×10^{-4} ($\pm 3 \times 10^{-5}$) for GB and 2×10^{-4} ($\pm 5.3 \times 10^{-5}$) for GD. The difference at an age of 380 Ma is 9.0×10^{-5} ($\pm 3 \times 10^{-5}$) for GB and 1.6×10^{-4} ($\pm 5.3 \times 10^{-5}$) for GD. For sample GA, the ^{87}Rb/^{86}Sr ratios of the segments are sufficiently different that the measured ^{87}Sr/^{86}Sr ratios do not increase from core to rim, but the age-corrected (~380 Ma) ratios do.

The calculated growth time intervals between the analyzed segments are 6.0 ± 2.6 m.y. for GB and 10.6 ± 4.1 m.y. for GD, for matrix II (Fig. 4). These time intervals correspond to average growth rates of $1.5^{+1.15}_{-0.44}$ mm/m.y. for GB and $1.1^{+0.7}_{-0.3}$ mm/m.y. for GD. Assuming constant radial growth rates and using the total radii of the garnets, we obtained total growth times of 10.0 ± 4.3 m.y. for GB and 12.7 ± 4.8 m.y. for GD. Using a model matrix that averages the ^{87}Rb/^{86}Sr ratios of matrix I and matrix II and setting the ^{87}Sr/^{86}Sr evolution line so that the age of the GA core is 380 Ma, we calculated that the time interval between GA-8 (core) and GA-4 is 6.6 ± 2.1 m.y. (Fig. 4). This gives an average growth rate of $1.7^{+0.9}_{-0.3}$ mm/m.y. and, extrapolated to the rim, a total growth time of 8.8 ± 3.6 m.y. The interval between GA-6 and GA-4 is 1.3 ± 2.2 m.y. The data for GA, although consistent with a constant radial growth rate within the uncertainties, hint that the outer portion of the garnet may have had a greater radial growth rate than the inner portion.

The apparent ages of the garnets calculated from segment-matrix pairs vary. The data imply that the garnets decrease in age in the order GD, GB, GA, with little overlap in growth interval (Figs. 4 and 5). The differences in calculated age either could be real or could result if the ^{87}Sr/^{86}Sr values of the matrix samples do not reflect precisely those from which the garnets actually grew. We prefer the latter interpretation because (i) it seems unlikely, although not inconceivable (*16*), that garnet crystals GB and GD, of similar diameter and separated by ~6 cm, would have nucleated 10 m.y. apart, and (ii) all of the absolute ages appear low in comparison with the nearby ^{40}Ar-^{39}Ar ages of 380 Ma, which may record a later stage in metamorphism. Most likely, GB and GD were in isotopic equilibrium with slightly different Sr reservoirs, and the analyzed matrix samples represent neither reservoir perfectly. It is also possible that matrix domains specific to individual garnets underwent differential modifications after garnet growth. The distance between GD and GB approximates the scale of Sr isotopic communication in the matrix during garnet growth. This isotopic variability apparently does not increase with increasing distance between samples because the initial isotopic difference between GB and GD cores (6-cm separation) is as great as that between GB and GA cores (1-m separation). This heterogeneity in the ^{87}Sr/^{86}Sr ratio may be an inherited variation of ^{87}Sr/^{86}Sr or ^{87}Rb/^{86}Sr ratios, or both, from the

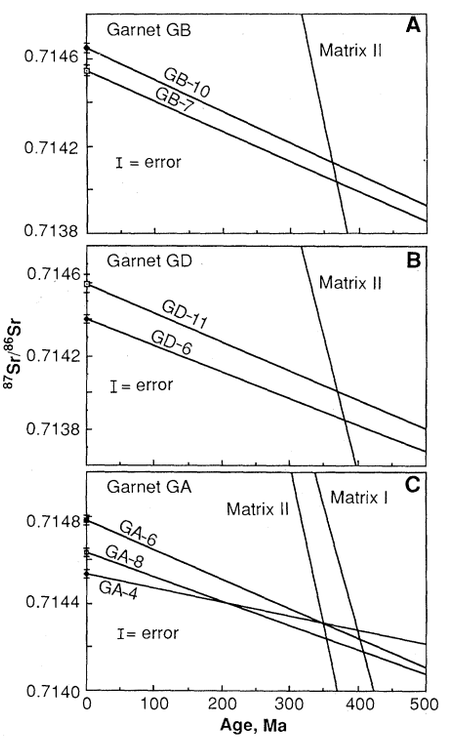

Fig. 3. Garnet and matrix ^{87}Sr/^{86}Sr evolution diagrams. (**A**) Garnet GB segments 7 and 10 (approximately core and rim) with matrix II; (**B**) garnet GD segments 6 and 11 (core and rim) with matrix II; (**C**) garnet GA segments 8, 6, and 4 (core, intermediate, and rim) with both matrix I and matrix II. Errors (Table 1) in the measured ^{87}Sr/^{86}Sr ratio are shown along the ordinate axis.

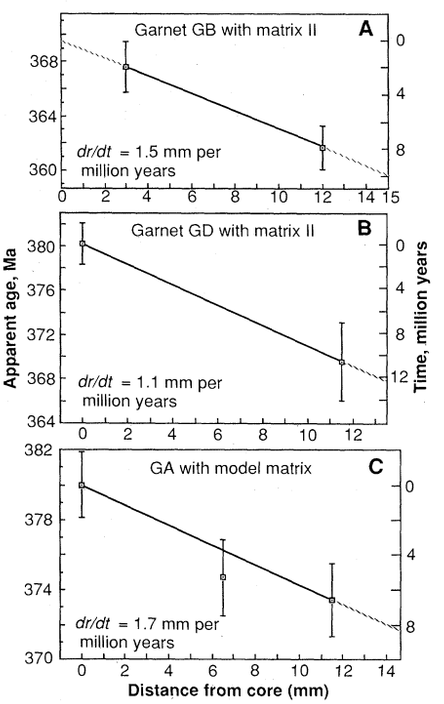

Fig. 4. Time versus distance core-to-rim plots for the analyzed garnets. (**A**) Garnet GB ages calculated with matrix II; (**B**) garnet GD ages calculated with matrix II; (**C**) garnet GA ages calculated with model matrix (average of matrix I and matrix II). Errors (at ~95% confidence level) in ages are calculated from the errors of the segment isotopic analyses and do not include the error of the matrix isotopic analysis.

sedimentary protolith.

As discussed above, the three remaining conditions (ii, iii, and iv) must be met for the determined growth intervals to be valid. The small scale of isotopic communication argues that the $^{87}Sr/^{86}Sr$ ratio of the matrix was not significantly influenced by infiltrating fluid, because that would be expected to cause isotopic homogenization on larger scales. The apparent small scale of isotopic communication casts doubt on whether a single garnet crystal, with a diameter of 3 cm, could be expected to sample a homogeneous reservoir during its growth. All the garnets, however, have initial $^{87}Sr/^{86}Sr$ ratios that increase from core to rim and that yield similar growth intervals and rates, suggesting satisfaction of the third requirement (*17*). Regarding the fourth condition, we estimate that the characteristic diffusive length scale for Sr in garnet for 10 m.y. at 500°C and a diffusivity of 10^{-20} cm^2/s (*18*) is about 3.5×10^{-2} mm, which is negligible relative to the diameters of the crystals. Diffusive effects would be important for small (millimeter-sized) garnets or garnets that were subjected to higher temperatures for a significant period of time.

The average growth rate of the three garnets ($1.4^{+0.92}_{-0.45}$ mm/m.y.) compares well with the range 10^3 to 1 mm/m.y. in growth rate estimated by Cashman and Ferry (*19*) for regional metamorphic garnets of south-central Maine using crystal size distributions and assumed reaction kinetics. The estimated total growth time for the small (~0.1 mm) garnets of that study was in the range <100 to 40,000 years, much shorter than that for GA, GB, and GD (average growth time = 10.5 ± 4.2 m.y.). In addition to the different sizes, the contrasting growth times may also reflect differing thermal histories; the proper conditions for garnet growth persisted for a longer period of time in the Vermont samples.

The average growth time allows calculation of average rates of deformation and heating during the growth of the garnets as the peak temperatures of metamorphism were approached. The spiral ("snowball") inclusion trails in GA indicate that it rotated ~4 radians during growth. For a simple shear approximation, the magnitude of the shear strain is twice the rotation angle (*7*) or ~8 over the growth time of the garnet. Growth of GA over an interval of 10.5 ± 4.2 m.y. leads then to an average shear strain rate of $2.4^{+1.6}_{-0.7} \times 10^{-14}$ s^{-1}. For an estimated shear stress of approximately 3 bars (*8*), the calculated strain rate corresponds to a viscosity of ~10^{20} poise.

For calculation of a heating rate, we estimate that the temperature of garnet nucleation was ~425°C on the basis of saturation compositions of both calcite coexisting with dolomite and muscovite coexisting with paragonite (*20*) for the rocks at the lowest temperature appearance of garnet in the area. The peak temperature was ~500°C on the basis of the $CaAl_2Si_2O_8$ content of plagioclase feldspar in a nearby sample (*7, 21*). This interval gives a heating rate of 5 to 10°C/m.y. during garnet growth, consistent with thermal modeling of orogenic belts (*22*).

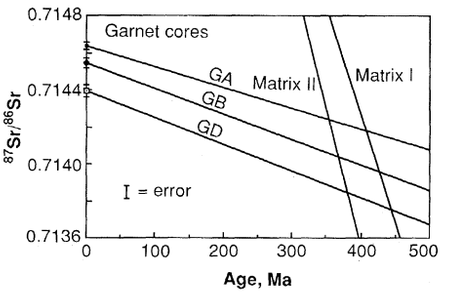

Fig. 5. $^{87}Sr/^{86}Sr$ evolution lines for cores of garnets GB, GD, and GA and, for reference, both matrix I and matrix II. Garnets GB and GD were ~3 cm apart, and garnet GA was ~1 m distant from the other two specimens.

Emplacement of the gneiss domes noted above folded the nappes while they were still hot. Sleep (*23*) used a thermal model for the relaxation of folded isotherms to constrain the duration of doming to ~1 m.y. The garnets we analyzed grew during the earlier nappe stage of deformation, whereas other garnets in different structural positions record both nappe- and dome-stage deformations (*8*). The doming event is recorded only in the outer 1 to 2 mm of these garnets. If a growth rate of 1.5 mm/m.y. also applies to the outer parts of these garnets, it implies that the dome stage deformation occurred on a time scale of ~1 m.y., in accord with Sleep's estimate (*23*). The total growth time of the analyzed garnets, which record nappe-stage deformation, constrains the total time allowed for the entire Acadian orogeny to be at least 10 m.y. This time span is a significant fraction of the ~30 m.y. between sedimentation and the end of Acadian deformation (*24*).

Our results suggest that this method may be generally applicable to rate studies in metamorphic terranes. Possible problems with the method concern the scale of isotopic homogeneity in the rock matrix and the size of the matrix volume sampled; furthermore, the volume sampled by a mineral will change during its growth. If further study bears out the applicability of the method, it should allow study of the kinetics of mineral growth and the determination of the timing and duration of deformation and heating at different structural levels of orogenic belts.

REFERENCES AND NOTES

1. Ratio of the numbers of atoms of the specified isotopes.
2. B. Yardley, *Am. Mineral.* **62**, 793 (1977).
3. M. R. St.-Onge, *J. Petrol.* **28**, 1 (1987).
4. H. G. Adams, L. H. Cohen, J. L. Rosenfeld, *Am. Mineral.* **60**, 584 (1975).
5. S. Hoernes and E. Hoffer, *ibid.* **68**, 377 (1979).
6. F. S. Spear and J. Selverstone, *Contrib. Mineral. Petrol.* **83**, 348 (1983).
7. J. L. Rosenfeld, *Geol. Soc. Am. Spec. Pap.* **129** (1970).
8. ———, in *Studies of Appalachian Geology: Northern and Maritime*, E. Zen, W. White, J. B. Hadley, J. B. Thompson, Jr., Eds. (Interscience, New York, 1968), pp. 185–202.
9. Equations 1 and 2 were derived from the decay equation in slope-intercept form first introduced by L. O. Nicolaysen [*Ann. N.Y. Acad. Sci.* **91**, 198 (1961)]; $\lambda = 1.42 \times 10^{-11}$ years^{-1}, the decay constant of ^{87}Rb [R. H. Steiger and E. Jäger, *Earth Planet Sci. Lett.* **36**, 359 (1977)].
10. The error dependency can be further illustrated with the approximation: $\ln(x + 1) \approx x$ when $x \ll 1$, which is a good approximation for our application. When applied to Eq. 2, this yields for the time interval of growth

$$t_2 - t_1 \approx \frac{S_2' - S_1'}{\lambda R_m} \approx \frac{S_2 - S_1}{\lambda R_m} - \frac{(t_2 R_2 - t_1 R_1)}{R_m}$$

For our application, $R_2 \approx R_1 \ll R_m$; thus the first and second terms of the right-hand side of the equation are of comparable magnitude. The uncertainty in the second term is typically about 1% (Table 1). The uncertainty in the first term is about 10 to 20% and lies almost entirely in the numerator $(S_2 - S_1)$ (Table 1). Hence, to a good approximation, the uncertainty in the age difference, $t_2 - t_1$, is determined by the uncertainty in the measured difference $S_2 - S_1$, which is much larger than all of the other uncertainties combined.
11. Nappes are asymmetric sheetlike recumbent folds $\gg$1 km in amplitude.
12. Though clinozoisite may contain >100 ppm Sr, the inclusions are in such low abundance (~0.01%) that they do not contribute greatly to the garnet Sr budget. Generally quartz, ilmenite, and tourmaline do not contain significant levels of Sr.
13. J. Laird *et al.*, *Am. J. Sci.* **284**, 376 (1984).
14. P. Karabinos and J. Laird, in *Guidebook for Field Trips, 80th New England Intercollegiate Geological Conference*, W. A. Bothner, Ed. (University of New Hampshire, Durham, 1988), pp. 281–292.
15. For analysis we crushed and dissolved approximately 150 mg of powdered matrix and 60 to 100 mg of garnet for each segment. Garnet dissolution was with hydrofluoric and perchloric acid in heated closed beakers. Matrix dissolution was similar except that a closed beaker was unnecessary. Because of the low Rb concentrations in garnet, we analyzed part of the solution for Rb by isotope dilution [see G. Faure, *Principles of Isotope Geology* (Wiley, New York, ed. 2, 1986)] before passing the remaining spiked sample through a cation exchange column to avoid the blank contribution to the Rb concentration. Total chemistry blanks were approximately 0.8 ng for Rb and 0.5 ng for Sr; Sr and Rb were separated with a cation exchange column devoted to the garnet samples. Isotopic analysis was done on a single-collector VG 54E mass spectrometer.
16. Several studies have concluded that nucleation and growth are continuous. Therefore crystals of similar size should have nucleated contemporaneously [see K. Jones and A. Galwey, *J. Geol. Soc. London* **122**, 29, 1966]. This assumption can be tested by analysis of coexisting garnets with recognizable time-correlative markers such as radial appearance or disappearance of a mineral from an inclusion suite [for example, C. Finlay and A. Kerr, *Contrib. Mineral. Petrol.* **71**, 185 (1979); also (*6*)] or a change in rotation axis during growth (*6, 7*).
17. Theories of metamorphic deformation and chemical reaction mechanisms suggest that, during metamorphism, the effective chemical diffusivities in rocks are much higher than measured volume diffusivities in

individual minerals would indicate. For example, textural evidence indicates that the chemical reaction that results in garnet growth involves repeated dissolution and reprecipitation of matrix minerals. The concurrent deformation also occurs partly by stress-solution: solution at grain interfaces under high normal compression and reprecipitation at interfaces under low normal compression. These processes repeatedly expose matrix grain interiors to the intergranular medium where diffusivities are higher than the corresponding volume diffusivities. [For more detailed discussion of supporting textural evidence, see J. L. Rosenfeld, in *Preferred Orientation in Deformed Metals and Rocks: An Introduction to Modern Texture Analysis*, H.-R. Wenk, Ed. (Academic Press, Orlando, FL, 1985), pp. 441–461, and D. M. Carmichael, *Contrib. Mineral. Petrol.* **20**, 244 (1969).]
18. The diffusivity of Sr is assumed not to exceed that of Mg in garnet as determined by R. T. Cygan and A. C. Lasaga [*Am. J. Sci.* **285**, 328 (1985)].
19. K. V. Cashman and J. M. Ferry, *Contrib. Mineral. Petrol.* **99**, 401 (1988).
20. J. L. Rosenfeld, *Am. J. Sci.* **267**, 343 (1969).
21. S. Maruyama, J. G. Liou, K. Suzuki, *Contrib. Mineral Petrol.* **81**, 268 (1982).
22. P. C. England and A. B. Thompson, *J. Petrol.* **25**, 894 (1984); A. B. Thompson and P. C. England, *ibid.*, p. 929 (1984).
23. N. H. Sleep, *J. Geol.* **87**, 583 (1979).
24. R. S. Naylor, *Science* **172**, 558 (1971).
25. We thank G. Bebout for help in the field and J. DeGrosse for his assistance in cutting and sectioning the garnets used in this study. This work was supported by NSF grant EAR87-07356 to J.L.R. and D.J.D., grant EAR 84-15143 to D.J.D., and grant 1601 to J.L.R. from the Committee on Research of the UCLA Academic Senate. G. Bebout, P. Bird, H. Reiss, and an anonymous reviewer provided critical comments on the manuscript.

8 February 1989; accepted 3 May 1989

Purification and Reconstitution of Chloride Channels from Kidney and Trachea

DONALD W. LANDRY,* MYLES H. AKABAS, CHRISTOPHER REDHEAD, ALEKSANDER EDELMAN,† EDWARD J. CRAGOE, JR.,‡ QAIS AL-AWQATI

Chloride channels mediate absorption and secretion of fluid in epithelia, and the regulation of these channels is now known to be defective in cystic fibrosis. Indanyloxyacetic acid 94 (IAA-94) is a high-affinity ligand for the chloride channel, and an affinity resin based on that structure was developed. Solubilized proteins from kidney and trachea membranes were applied to the affinity matrix, and four proteins with apparent molecular masses of 97, 64, 40, and 27 kilodaltons were eluted from the column by excess IAA-94. A potential-dependent $^{36}Cl^-$ uptake was observed after reconstituting these proteins into liposomes. Three types of chloride channels with single-channel conductances of 26, 100, and 400 picosiemens were observed after fusion of these liposomes with planar lipid bilayers. Similar types of chloride channels have been observed in epithelia.

CHLORIDE CHANNELS ARE PRESENT in the plasma membrane of most cells. In epithelia these channels act together with other ion transporters, such as the $Na^+,K^+,2Cl^-$cotransporter and the Na^+- and K^+-dependent adenosine triphosphatase, to mediate absorption or secretion of NaCl (*1*). Characterization of the channels has been limited to analysis of electrophysiological properties such as single-channel conductance, voltage dependence, and the effect of second messengers on channel opening. In airway epithelia the opening of a channel with a conductance of 40 to 50 pS and a rectifying current-voltage (*I-V*) relation was stimulated by the adenosine 3′,5′-monophosphate–dependent protein kinase (A-kinase) (*2*). The inability of A-kinase to stimulate channel opening in excised apical membrane patches of secretory cells is thought to reflect the pathogenetic defect in cystic fibrosis (*2*). Similar Cl^- channels are present in fibroblasts and lymphocytes, and here too their opening is defective in cystic fibrosis (*3*).

We have developed high-affinity ligands for the Cl^- channel by screening inhibitors of $^{36}Cl^-$ transport in bovine kidney cortex microsomes (*4*). An indanyloxyacetic acid, IAA-94 (Fig. 1), was the most potent inhibitor with an inhibition constant (K_i) of 1 μ*M*, and [^{3}H]IAA-94 bound to these microsomes with a dissociation constant (K_d) of 0.6 μ*M*. Similar results were seen in apical membranes from bovine trachea. The rank order of potency for inhibition of $^{36}Cl^-$ transport for several inhibitors correlated with that for displacement of [^{3}H]IAA-94, suggesting that IAA-94 binds to the Cl^- channel. We describe here the purification of the solubilized channel by chromatography on an affinity matrix based on the IAA structure. Reconstitution of the purified proteins into planar bilayers revealed the presence of Cl^- channels.

To purify Cl^- channels from bovine kidney cortex vesicles and from apical membranes of bovine trachea, we first solubilized these preparations in *n*-octyl glucoside. A final detergent concentration of 1.4% solubilized 60% of the protein and 20% of the [^{3}H]IAA-94 binding sites (*5*). The addition of 10% glycerin preserved the number of solubilized binding sites after freezing at −70°C or incubation at 4°C for 24 hours. The concentration of IAA-94 required to displace 50% of the specifically bound ^{3}H-labeled ligand (IC_{50}) from the solubilized proteins was 2 μ*M*, similar to the value obtained for intact vesicles. Potential-driven $^{36}Cl^-$ uptake was observed when the solubi-

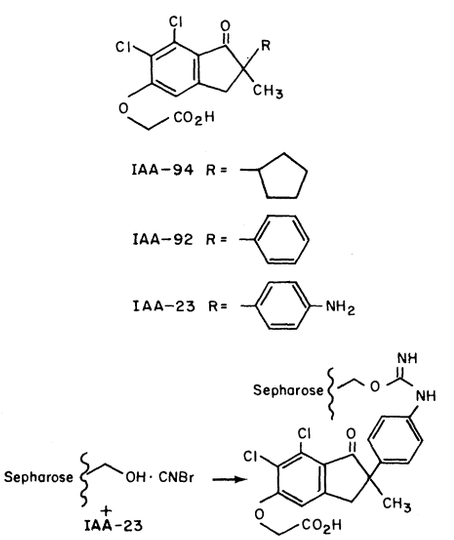

Fig. 1. Structures of IAA and synthesis of the affinity resin. Dry cyanogen bromide (CNBr)–activated Sepharose 4B was reswollen with ice-cold HCl (1 m*M*). After 15 min the resin was washed with a solution containing 0.1*M* $NaHCO_3$ and 0.5*M* NaCl (*p*H 9). The IAA-23 was dissolved in 0.1*M* $NaHCO_3$ and 0.5*M* NaCl (*p*H 9) and added to the swollen resin (1.5 μmol of IAA-23 per milliliter of resin). The mixture was agitated at room temperature for 48 hours. Depletion of the ligand from the supernatant was followed by ultraviolet spectroscopy at a wavelength of 268 nm. The efficiency of depletion averaged 97%. The resin was washed by alternating 0.1*N* tris (*p*H 8.5) and 0.1*N* sodium acetate (*p*H 4.5) and then stored in a solution containing 250 m*M* sucrose, 10 m*M* imidazole (*p*H 7), and 0.02% NaN_3. Before use the resin was washed with a solution containing 250 m*M* sucrose, 10 m*M* imidazole (*p*H 6.0), 10% glycerin, and 1.4% *n*-octyl glucoside.

D. W. Landry, M. H. Akabas, C. Redhead, A. Edelman, Q. Al-Awqati, Departments of Medicine and Physiology, College of Physicians and Surgeons, Columbia University, New York, NY 10032.
E. J. Cragoe, Jr., Merck Sharp and Dohme Research Laboratories, West Point, PA 19486.

*To whom correspondence should be addressed.
†Permanent address: INSERM, Unite 192, Paris, France.
‡Present address: 2211 Oak Terrace Drive, Lansdale, PA 19446.